Proceedings of the ASME 2010 3rd Joint US-European Fluids Engineering Summer Meeting and 8th International Conference on Nanochannels, Microchannels, and Minichannels
FEDSM-ICNMM2010
August 1-5, 2010, Montreal, Canada

FEDSM-ICNMM2010-31129

MODELING LAMINAR FLUID FLOWS IN RECTANGULAR VAPOR GROOVES OF EVAPORATORS USED IN LOOP HEAT PIPES

Nirmalakanth Jesuthasan
Heat Transfer Laboratory
Department of Mechanical Engineering
McGill University
Montreal, Quebec, Canada

B. Rabi Baliga
Heat Transfer Laboratory
Department of Mechanical Engineering
McGill University
Montreal, Quebec, Canada

ABSTRACT

Loop heat pipes (LHPs) are devices in which capillary forces in a wick and liquid-vapor phase-change phenomena are used to achieve continuous and relatively high rates of transfer of thermal energy from a heat source to a heat sink. Quasi one-dimensional models of the fluid flow and heat transfer within LHPs, with empirical correlations as inputs, are commonly used as the basis of cost-effective computer simulations for the design and optimization of these devices for specific applications. The focus in this work is on laminar fluid flows in straight rectangular vapor grooves of flat evaporators used in LHPs. The pressure drops for such fluid flows are computed in available quasi one-dimensional models of LHPs using correlations for a friction factor that applies strictly only in the fully-developed region of flows in straight rectangular ducts with impermeable walls. The resulting errors can become serious if the pressure drop in the vapor grooves is a significant contributor to the overall pressure drop in the LHP. Thus, to enhance the capabilities of current quasi one-dimensional models of LHPs, more accurate correlations for predicting the aforementioned pressure drop are needed. In this work, a three-dimensional parabolic finite volume method is used to simulate laminar Newtonian fluid flows in straight rectangular vapor grooves of flat evaporators, for a representative range of LHP operating conditions. The mathematical model, computational methodology, results, and suitable correlations for the pressure drops are presented and discussed in this paper.

INTRODUCTION

Loop heat pipes (LHPs) are devices in which capillary forces in a wick and liquid-vapor phase-change phenomena are used to achieve continuous transfer of thermal energy from a heat source to a heat sink, with no mechanical moving parts, no special external power inputs, and relatively small temperature drops over long distances. Furthermore, the heat transfer rates that are achievable with LHPs are typically one to three orders of magnitude larger than those possible with either single-phase convection systems or solid thermal conductors for corresponding thermal boundary conditions. For these reasons, since the invention of LHPs in the former Soviet Union in the 1970s, there has been a great deal of interest in mathematical models of these devices and also their applications in a multitude of heat-exchange systems. In particular, quasi one-dimensional models of the fluid flow and heat transfer within LHPs, with empirical correlations as inputs, are commonly used as the basis of cost-effective computer simulations for the design and optimization of these devices for specific applications. Detailed descriptions and reviews of LHPs are available in Chi (1976), Silverstein (1992), Faghri (1995), Maydanik (2005), Launay et al. (2007), Vlassov and Riehl (2008), and Vasiliev et al. (2009), for example.

The focus in this work is on laminar flow of vapor in straight rectangular grooves of flat evaporators used in LHPs, similar to those shown schematically in Figure 1. The problems of interest can be modeled as flows in a straight rectangular duct with one end blocked and a uniform (or average) injection velocity, v_{inj}, imposed on the bottom lateral surface, as shown schematically in Figure 2. The pressure drops for such fluid flows are computed in available quasi one-dimensional models of LHPs using correlations for a friction factor that applies strictly only in the fully-developed regions of flows in straight rectangular ducts with impermeable walls [Kaya and Hoang (1999); Maydanik (2005); Atabaki (2006); Atabaki et al. (2007); Launay et al. (2007)]. This approach is inapplicable or ad hoc, at best, with respect to the vapor flows illustrated in Figure 2. The resulting errors can become serious if the pressure drop in the vapor grooves is a significant contributor to the overall pressure drop in the LHP. Thus, to enhance the

capabilities of current quasi one-dimensional models of LHPs, more accurate correlations for predicting the aforementioned pressure drop are needed.

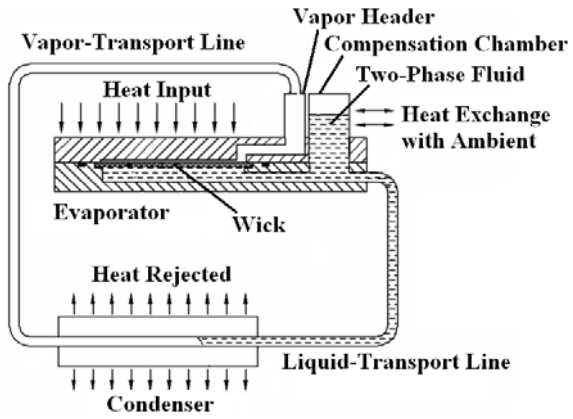

(a)

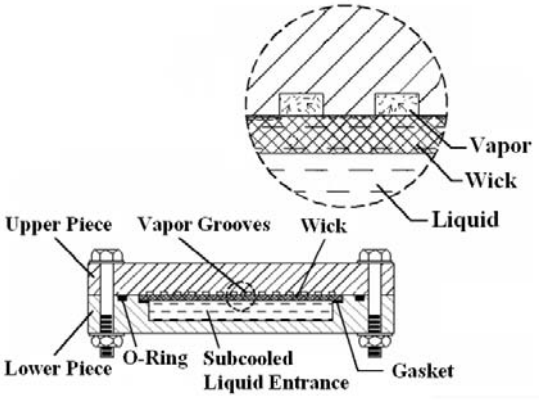

(b)

Figure 1: (a) schematic representation (not to scale) of a loop heat pipe with a flat evaporator; and (b) details of the flat evaporator section.

In the published literature, there are many papers related to laminar fluid flows in straight ducts with an inlet velocity imposed at one end, blowing or suction along one or more lateral surfaces, and an outflow condition at the other end: examples include the works of Berman (1953), Taylor (1956), Yuan and Finkelstein (1958), Kinney (1968), Bundy and Weissberg (1970), Pederson and Kinney (1971), Raithby (1971), Raithby and Knudsen (1974), Rhee and Edwards (1981), Ku and Leidenfrost (1981), Hwang et al. (1993), Yuan et al. (2001), and Beale (2005). In the vapor flows of interest, however, as shown schematically in Figure 2, one end of the rectangular duct is blocked (there is no inlet velocity at this end). Furthermore, in the aforementioned works, there are no correlations that can be readily adapted for accurate application in quasi one-dimensional models of LHPs. There are also many published papers on vapor flows in heat pipes, akin to that shown schematically in Figure 3: examples include the works of Busse (1967, 1973), Tien and Rohani (1974), Chen and Faghri (1990), and Leong et al. (1996). However, in the vapor flow passage of heat pipes, both ends are blocked and there is blowing and suction along the lateral surface, as is clear from the schematic in Figure 3, and these boundary conditions are not the same as those in the vapor flow grooves of LHP evaporators (Figure 2). In this work, a three-dimensional parabolic finite volume method is used to simulate laminar Newtonian fluid flows akin to that shown schematically in Figure 2, for parameter ranges representative of LHP operating conditions. The mathematical model, computational methodology, results, and suitable correlations for the pressure drops are presented and discussed in this paper.

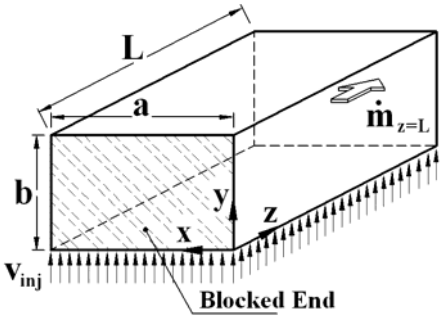

(a)

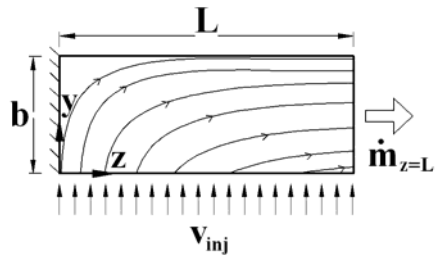

(b)

Figure 2: (a) schematic representation of vapor flow in rectangular grooves of a flat evaporator of an LHP; (b) cross-sectional (y-z plane) view of this flow.

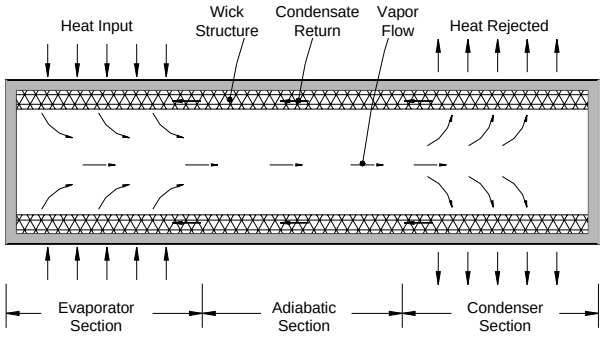

Figure 3: Schematic representation of a typical heat pipe [Atabaki (2006)].

NOMENCLATURE

A_{c-s}	cross-sectional area (= ab) of the duct, Figure 2
AR	aspect ratio (= a/b) of duct cross-section, Figure 2
D_h	hydraulic diameter, equation (10)
f	friction factor, equation (14)
f_{app}	apparent friction factor, equation (16)
$\dot{m}$	total mass flow rate at *z*, equation (8)
p	perturbation pressure, equation (1)
p^*	dimensionless *p*, equation (3)
P	reduced pressure
$\overline{P}$	cross-sectional average value of *P*, equation (1)
$\overline{P}^*$	dimensionless $\overline{P}$, equation (3)
Re_{D_h}	Reynolds number at *z*, equation (12)
Re_{inj}	injection Reynolds number, equation (3)
u, v, w	components of the velocity in the *x*, *y*, and *z* directions, respectively
v_{inj}	injection velocity, Figure 2
U, V, W	dimensionless forms of *u*, *v*, *w*, equation (3)
w_{av}	cross-sectional average value of *w*, equation (8)
W_{av}	dimensionless form of w_{av}, equation (8)
x, y, z	Cartesian coordinate directions, Figure 2
X, Y, Z	dimensionless forms of *x*, *y*, *z*, equation (3)
z^+	dimensionless z (= $(z/D_h)/\mathrm{Re}_{D_h}$)
Z^+	dimensionless z, equation (13)

Greek symbols

α	under-relaxation factors
μ	fluid dynamic viscosity
ρ	fluid mass density

Subscripts

av	cross-sectional average value
F.D.	pertaining to the full-developed region
inj	pertaining to injection

MATHEMATICAL MODEL

In the range of operating conditions of the LHPs considered in this work, the geometry of the vapor grooves in the flat evaporator and the magnitude of the flow rate in them are such that the corresponding Reynolds number based on the maximum value of the mean velocity and the hydraulic diameter is 2000 or lower, so the flow remains laminar throughout. The vapor is assumed to be a Newtonian fluid with constant density and dynamic viscosity (evaluated at the average values of the pressure and bulk temperature). For any specified overall rate of heat input, the temperature, T_w, of the upper half of the metallic flat evaporator body, which houses the rectangular vapor grooves (see Figure 1), is essentially constant. Furthermore, the total pressure drop in the vapor grooves is typically a relatively small fraction of the average absolute pressure. Thus, the saturation temperature, T_{sat}, at the liquid-vapor interface adjacent to the upper surface of the wick (see Figure 1) and the temperature difference ($T_w - T_{sat}$) that drives the phase-change process are essentially constant. Therefore, the mass flux of the vapor and the corresponding injection velocity, v_{inj}, on the bottom surface of each groove may be considered to be essentially uniform.

The following additional assumptions are also invoked: the vapor flow is steady; there exists a predominant flow along the vapor groove, and no flow reversal is encountered in that direction; the diffusion (or viscous) transport in the mainstream direction is negligible compared to the corresponding advection transport and the cross-stream diffusion transport; and the downstream pressure field has negligible influence on the upstream flow conditions. With these assumptions, the vapor flows of interest in this work can be characterized as three-dimensional parabolic, as discussed in the seminal work of Patankar and Spalding (1972).

With reference to the Cartesian coordinate system and notation shown in Figure 2, the components of the velocity vector in the *x*, *y*, and *z* directions are denoted by *u*, *v*, and *w*, respectively. The symbols ρ and μ are used to denote the mass density and dynamic viscosity of the fluid, respectively. The reduced pressure is denoted by *P*, and following Patankar and Spalding (1972), it is expressed in terms of its cross-sectional average value, $\overline{P}$, and a perturbation component about this average, *p*, as follows:

$$P(x,y,z) = \overline{P}(z) + p(x,y,z);\ \overline{P}(z) = \frac{1}{A_{c-s}} \int_{A_{c-s}} P(x,y,z)\,dxdy \quad (1)$$

In this equation, A_{c-s} is the cross-sectional area of the duct. Again following Patankar and Spalding (1972), it is assumed that $(\partial p/\partial z) << d\overline{P}/dz$, and the following approximation and expressions apply:

$$\partial P/\partial z = d\overline{P}/dz;\ \partial P/\partial x = \partial p/\partial x;\ \partial P/\partial y = \partial p/\partial y \quad (2)$$

At this stage, with reference to the Cartesian coordinate system and notation shown in Figure 2, the following dimensionless variables and parameters are introduced:

$$\begin{aligned} &X = x/b;\ Y = y/b;\ Z = z/b;\ AR = a/b \\ &U = u/v_{inj};\ V = v/v_{inj};\ W = w/v_{inj} \\ &p^* = p/(0.5\rho v_{inj}^2);\ \overline{P}^* = \overline{P}/(0.5\rho v_{inj}^2);\ \mathrm{Re}_{inj} = \rho v_{inj} b/\mu \end{aligned} \quad (3)$$

Here, *AR* is the aspect ratio of the rectangular cross-section of the duct, and Re_{inj} is the injection Reynolds number. In the context of the aforementioned assumptions and in terms of the dimensionless variables and parameters given in equation (3), the differential equations that govern the vapor flows of interest can be cast in the following forms [Patankar and Spalding (1972); Jesuthasan and Baliga (2009)]:

Continuity:

$$\frac{\partial U}{\partial X}+\frac{\partial V}{\partial Y}+\frac{\partial W}{\partial Z}=0 \tag{4}$$

x-momentum:

$$\frac{\partial}{\partial X}(UU)+\frac{\partial}{\partial Y}(VU)+\frac{\partial}{\partial Z}(WU)= -\frac{\partial p^*}{\partial X}+\frac{1}{\mathrm{Re}_{inj}}\left(\frac{\partial^2 U}{\partial X^2}+\frac{\partial^2 U}{\partial Y^2}\right) \tag{5}$$

y-momentum:

$$\frac{\partial}{\partial X}(UV)+\frac{\partial}{\partial Y}(VV)+\frac{\partial}{\partial Z}(WV)= -\frac{\partial p^*}{\partial Y}+\frac{1}{\mathrm{Re}_{inj}}\left(\frac{\partial^2 V}{\partial X^2}+\frac{\partial^2 V}{\partial Y^2}\right) \tag{6}$$

z-momentum:

$$\frac{\partial}{\partial X}(UW)+\frac{\partial}{\partial Y}(VW)+\frac{\partial}{\partial Z}(WW)= -\frac{d\bar{P}^*}{dZ}+\frac{1}{\mathrm{Re}_{inj}}\left(\frac{\partial^2 W}{\partial X^2}+\frac{\partial^2 W}{\partial Y^2}\right) \tag{7}$$

In addition to the above-mentioned equations, the overall or total mass flow rate through the duct at each value of the main-stream coordinate (z) must be respected. With reference to the notation given in Figure 2, and with the assumption of uniform injection velocity, v_{inj}, this mass flow rate is given by the following equation:

$$\dot{m}=\int_{A_{c-s}} \rho w dA_{c-s}=\rho(az)v_{inj}=\rho(ab)w_{av}, \text{ or}$$
$$W_{av}=w_{av}/v_{inj}=(z/b)=Z \tag{8}$$

The five equations (4) to (8) form a parabolic system in the main-stream coordinate direction, Z, with five unknowns, U, V, W, p^*, and $(-d\bar{P}^*/dZ)$. To specify the problem completely, the boundary conditions and the dimensionless parameters (AR and Re_{inj}) must be specified. Once the problem description is complete, the parabolic model allows a marching solution procedure in the Z direction, so the solution can be advanced step-by-step along the duct, from $Z = 0$ to $Z = L/b$, as described in detail in the seminal work of Patankar and Spalding (1972) and also in the recent work of Jesuthasan and Baliga (2009).

In this work, with respect to the problem schematic given in Figure 2(a), and the dimensionless variables and parameters given in equation (3), the following boundary conditions apply:

$$\begin{aligned}
&\text{At } X=0,\ U=V=W=0\\
&\text{At } X=0.5AR,\ U=0;\ \partial V/\partial X=\partial W/\partial X=0\\
&\text{At } Y=0,\ U=V=W=0\\
&\text{At } Y=1,\ U=V=W=0\\
&\text{At } Z=0,\ U=V=W=0,\ \bar{P}^*=\bar{P}^*_{ref}\\
&\text{At } X=Y=0,\ p=p^*_{ref}
\end{aligned} \tag{9}$$

The boundary conditions at $X = 0.5AR$ correspond to the longitudinal, vertical, symmetry surface at that location. In the parabolic mathematical model, in the main-stream direction, boundary conditions are needed only at $Z = 0$. With respect to the boundary conditions on $\bar{P}^*$ and p^*, as the fluid density (ρ) is assumed to be essentially constant, only the drops in the fluid pressure (that drive the fluid flow) matter, and not its absolute value [Patankar (1980)]. In the proposed parabolic model, as is indicated in equation (9), the values of dimensionless cross-sectional average and perturbation pressures are assigned suitable reference values ($\bar{P}_{ref}$ and p^*_{ref}) at the convenient locations $Z = 0$, and $X = Y = 0$.

NUMERICAL SOLUTION METHOD

A co-located finite volume method (FVM) was used to solve the three-dimensional parabolic mathematical model described in the previous section. It incorporates key concepts borrowed from the seminal and well-established three-dimensional parabolic, staggered-grid, FVM of Patankar and Spalding (1972). Its formulation is closely related to that of the three-dimensional parabolic, co-located, control-volume finite element method (CVFEM) of Jesuthasan and Baliga (2009), and the two-dimensional elliptic, co-located, FVM described by Baliga and Atabaki (2006). As full details of these numerical methods are available in the aforementioned references, only a very brief overview of the main features of the FVM used in this work are presented in this section.

In the three-dimensional parabolic FVM used in this work, a step-by-step marching procedure in the axial direction is used to solve the problems of interest, from the $Z = 0$ to $Z = L/b$ (the exit plane of the duct). In each step, the solution is advanced from an upstream cross-section of the duct, located at Z, to the next downstream cross-section, located at $Z + \Delta Z$. Each cross-section (X-Y plane) of the duct is first discretized into contiguous rectangular control volumes that fill the domain exactly. Then, nodes or grid points are located at the geometric centers of the control volumes, the centers of the control volume faces that coincide with the boundaries of the domain, and the corners of rectangular domain. The grid points or nodes lie on lines that are parallel to the coordinate axes, and these grid lines could be non-uniformly spaced. This discretization of the duct cross-section is illustrated in Figure 4. The boundaries of the cross-sectional control volumes associated with corresponding pairs of upstream and downstream nodes are joined to form rectangular parallelepiped control volumes of extents ΔX,

ΔY, and ΔZ in the *X*, *Y*, and *Z* coordinate directions, respectively. All dependent variables and the fluid thermophysical properties are stored at the same set of nodes (co-located formulation) in the upstream (*Z*) and downstream ($Z + \Delta Z$) cross-sections.

The governing differential equations are first integrated over the control volumes, and algebraic approximations to the integral conservation equations are then derived. These algebraic approximations are called the discretized equations. In the derivation of these discretized equations, the *X*- and *Y*-direction advection and diffusion transport terms are discretized using the hybrid scheme [Patankar (1980)], which is second-order accurate at low velocities (strictly, at grid Peclet number values less than 2) and uniform grids; and a second-order quadratic interpolation is used at the cross-sectional boundaries, and appropriately adjusted to incorporate the specified boundary conditions [Baliga and Atabaki (2006)]. The reduced perturbation pressure, p^*, in the cross-section (*X*-*Y* plane) is interpolated using piecewise-linear functions between the nodes. In the mass flow rate terms, the *U* and *V* velocity components are interpolated using the so-called momentum interpolation scheme [Rhie and Chow (1983)], to avoid undesirable checkerboard-type pressure and velocity distributions that would otherwise afflict this equal-order co-located FVM [Patankar (1980)]. In the *X*-*Y* plane, the nodal values of ρ and μ are interpolated to locations where the grid lines intersect the control-volume faces, using a resistance analogy (which reduces to the harmonic mean on uniform grids), as described in Patankar (1980). In this work, however, this is a moot point as ρ and μ are assumed to stay essentially constant. In the main-stream (*Z*) direction, a fully-implicit discretization scheme is used [Patankar (1980)] at each axial step, ΔZ.

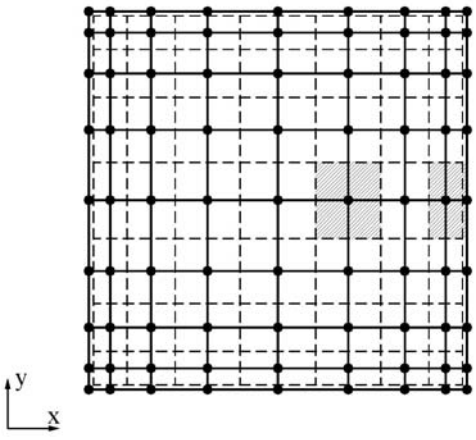

Figure 4: Discretization of a rectangular cross-section of the duct at each axial (*z*) location: dashed lines indicate control volume faces; solid dots indicate nodes or grid points; solid lines denote grid lines; and the hashed regions show two control volumes, one in the domain interior and the other adjacent to its boundary.

To advance the solution from an upstream cross-section at *Z* to the next downstream cross-section at $Z + \Delta Z$, an overall sequential iterative solution procedure was used to solve the nonlinear coupled discretized equations. This procedure incorporates elements of the sequential iterative variable adjustment (SIVA) procedure proposed by Saabas and Baliga (1994) and the semi-implicit method for pressure-linked equations revised (SIMPLER) of Patankar (1980). In each overall iteration of this procedure, decoupled and linearized sets of the discretized equations for *U*, *V*, *W*, and p^* were solved iteratively using a line-Gauss-Seidel method. Full details of this method are available in the works of Patankar (1980), and Sebben and Baliga (1995).The discretized equations for *U*, *V*, and p^* were under-relaxed using an implicit scheme proposed by Patankar (1980), with the following under-relaxation factors: $\alpha_U = \alpha_V = 0.8$, and $\alpha_{p^*} = 1.0$; no under-relaxation was used or necessary in the solution of the discretized equations for *W* and $d\bar{P}^*/dZ$. At each axial step, convergence of the aforementioned overall sequential iterative solution procedure was assumed to be achieved when suitably normalized absolute residues of the discretized equations for the dependent variables were all less than 10^{-4}.

Before using the aforementioned three-dimensional parabolic FVM to investigate the fluid flows of interest, its validity was established by applying it to developing laminar flow in straight ducts of rectangular cross-section, with *impermeable* walls and aspect ratio *AR* = 1 and 5, and comparing the results to the corresponding numerical solutions given in Curr et al. (1972) and Shah and London (1978). Results obtained with uniform grids of 21 x 21, 41 x 41, 61 x 61, and 81 x 81 nodes in the full extent of the cross-sectional plane (*X*-*Y*), and dimensionless axial step sizes of $\Delta z^+ = \Delta\{(z/D_h)/\mathrm{Re}_{D_h}\}$ = 1 x 10^{-3}, 5 x 10^{-4}, and 5 x 10^{-5}, were used in these comparisons. Here, $\mathrm{Re}_{D_h} = \rho w_{av} D_h / \mu$ is the Reynolds number, w_{av} is the average axial velocity of the fluid in the duct cross-section, and D_h is the hydraulic diameter:

$$D_h = 4ab/[2(a+b)] = [2AR/(1+AR)]b \qquad (10)$$

Predictions yielded by the aforementioned FVM for the variation of $f_{app}\,\mathrm{Re}_{D_h} = \left\{(\bar{P}_{z=0} - \bar{P}_z)/z\right\} D_h \Big/ \left\{0.5\rho w_{av}^2\right\} \mathrm{Re}_{D_h}$ with z^+, with uniform cross-sectional grids of 21 x 21, 41 x 41, 61 x 61, and 81 x 81 nodes, and Δz^+ = 5 x 10^{-5}, and also the results of Curr et al (1972), are given in Figure 5, for *AR* = 1 and 5. These plots show that the results yielded by the 41 x 41, 61 x 61, and 81 x 81 cross-sectional grids essentially coincide (within the resolution of the plots) and compare very well with the results of Curr et al (1972): quantitatively, the maximum percentage absolute differences between the results yielded by the cross-sectional grids of 41 x 41 and 81 x 81 nodes were 0.156% and 1.09% for *AR* = 1 and 5, respectively; and the maximum

percentage absolute differences between the results yielded by the cross-sectional grid of 41 x 41 nodes and those of Curr et al. (1972) were 0.97% for both of the aforementioned values of *AR*. The same results yielded by the FVM with a cross-sectional grid of 41 x 41 nodes and $\Delta z^+ = 1 \times 10^{-3}$, 5×10^{-4}, and 5×10^{-5} are shown in Figure 6 for *AR* = 1, along with the results of Curr et al. (1972): the maximum percentage absolute difference between the results obtained with $\Delta z^+ = 1 \times 10^{-3}$ and 5×10^{-5} was 1.72%; and, as was stated earlier, the maximum percentage absolute difference between the results obtained with $\Delta z^+ = 5 \times 10^{-5}$ and those of Curr et al. (1972) was 0.97%.

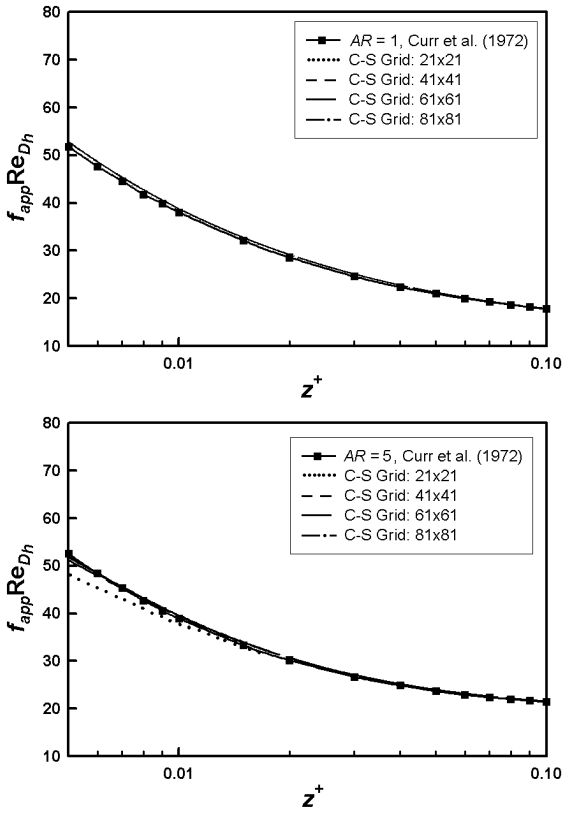

Figure 5: Variations of $f_{app}\,\mathrm{Re}_{D_h}$ with z^+ for developing laminar flow in straight ducts of rectangular cross-section, with impermeable walls and aspect ratio *AR* = 1 and 5: FVM results obtained with four different cross-sectional grids and $\Delta z^+ = 5 \times 10^{-5}$; and the results of Curr et al. (1972).

The FVM predictions for developing laminar flow in a straight duct of square cross-section (*AR* = 1) and impermeable walls, obtained with a uniform cross-sectional grid of 41 x 41 nodes and $\Delta z^+ = 5 \times 10^{-5}$, were also in excellent agreement with the experimental results of Goldstein and Kreid (1967) and Beavers et al. (1970), as shown by the plots in Figure 7. Quantitatively, the absolute differences between the FVM predictions and the corresponding experimental results were well within the error bands reported by Goldstein and Kreid (1967) and Beavers et al. (1970).

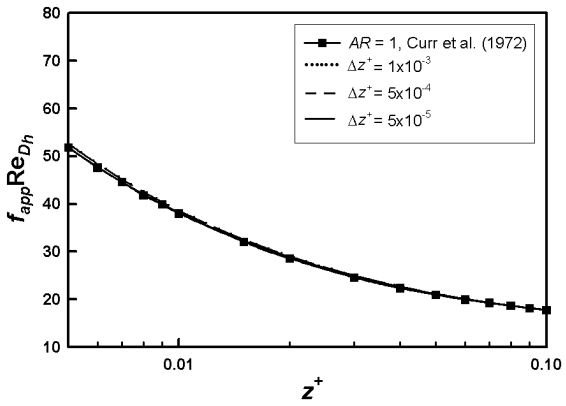

Figure 6: Variations of $f_{app}\,\mathrm{Re}_{D_h}$ with z^+ for developing laminar flow in straight ducts of rectangular cross-section, with impermeable walls and aspect ratio *AR* = 1: FVM results obtained with a cross-sectional grid of 41 x 41 nodes and three different values of Δz^+; and the results of Curr et al. (1972).

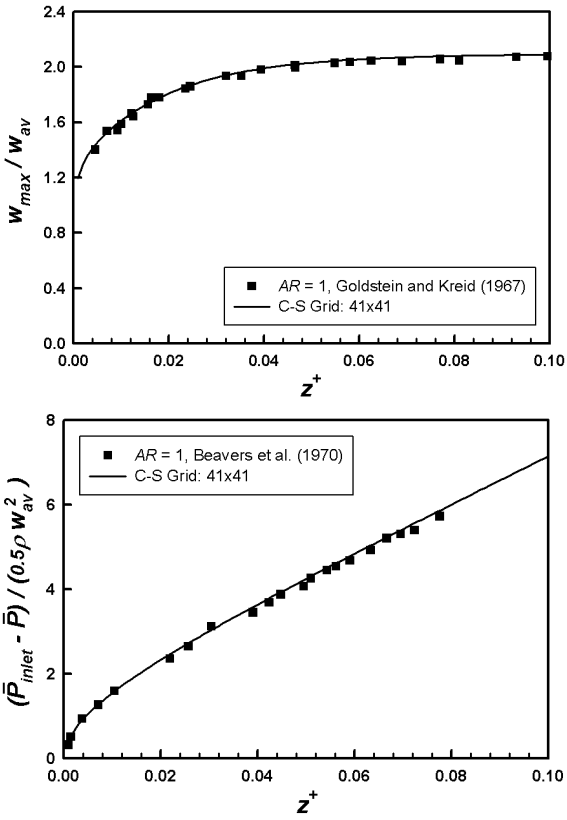

Figure 7: Variations of $(w_{\max} / w_{av})$ and $(\bar{P}_{inlet} - \bar{P})/(0.5\rho w_{av}^2)$ with z^+ for developing laminar flow in straight ducts of rectangular cross-section, with impermeable walls and aspect ratio *AR* = 1: FVM results obtained with a cross-sectional grid of 41 x 41 nodes and $\Delta z^+ = 5 \times 10^{-5}$; and the experimental results of Goldstein and Kreid (1967) and Beavers et al. (1970).

The results presented in Figures 5 – 7 confirm the consistency and validity of the FVM.

RESULTS AND DISCUSSIONS

The problems of interest involve laminar fluid flows in straight vapor groves of rectangular cross-section in flat evaporators of loop heat pipes (LHPs), akin to the one shown schematically in Figure 1. The schematic representation of such a flow in one rectangular vapor groove is shown in Figure 2. Keeping practical applications in mind, the following values of the dimensionless parameters, AR and Re_{inj}, were considered in this work:

$$\begin{aligned} &AR = 1,\ 2,\ \text{and}\ 5 \\ &AR \times \mathrm{Re}_{inj} = 0.1,\ 1,\ 10,\ \text{and}\ 100 \end{aligned} \qquad (11)$$

In the longitudinal direction of the duct, with uniform rate of injection into the duct (v_{inj} = constant), the mass flow rate increases linearly with z, as shown by the expression given earlier in equation (8). Thus, in each of the 12 cases investigated, to ensure that the fluid flow remained laminar throughout the duct, the local value of the Reynolds number, Re_{D_h}, based on the average value of the axial velocity, w_{av}, and the hydraulic diameter, D_h, at the exit plane ($z = L$) was limited to 2000. Thus, using the expressions for w_{av} and D_h given in equations (8) and (10), respectively,

$$\mathrm{Re}_{D_h} = \frac{\rho w_{av} D_h}{\mu} = \frac{\rho[(z/b)v_{inj}][2AR/(1+AR)]b}{\mu} \le 2000 \qquad (12)$$

In terms of the injection Reynold number, Re_{inj}, and the dimensionless variable Z defined in equation (3), equation (12) can be expressed as follows:

$$Z^+ = \left(\frac{z}{b}\right)\left(\frac{2AR}{1+AR}\right)\left(\frac{\rho v_{inj} b}{\mu}\right) = Z\left(\frac{2AR}{1+AR}\right)\mathrm{Re}_{inj} \le 2000 \qquad (13)$$

In the light of this equation, the local Reynolds number, Re_{D_h}, can be interpreted as a new dimensionless axial coordinate, Z^+, for the fluid flows of interest (see Figure 2). It should be noted that Z^+ is different from the dimensionless axial coordinate $z^+ = Z/\mathrm{Re}_{D_h}$ which is used in the mathematical description of developing fluid flows in straight ducts with impermeable walls. In this work, for each case of interest, the computations were carried out in the region $0 \le Z^+ \le 2000$.

The seminal works of Berman (1953), and Yuan and Finkelstein (1958) have shown that steady laminar flows in straight ducts with uniform injection from one or more longitudinal walls become fully developed after a sufficient longitudinal distance from the inlet plane, in the sense that the velocity components normalized with respect to the *local* longitudinal average velocity, w_{av}, become invariant with the axial coordinate, z. Taking guidance from these works, it was expected that the flows of interest (see schematic in Figure 2) would also be come fully developed after a sufficient longitudinal distance from the blocked end (at z = 0) of the duct. The numerical results of this investigation confirmed these expectations, as will be discussed later in this section.

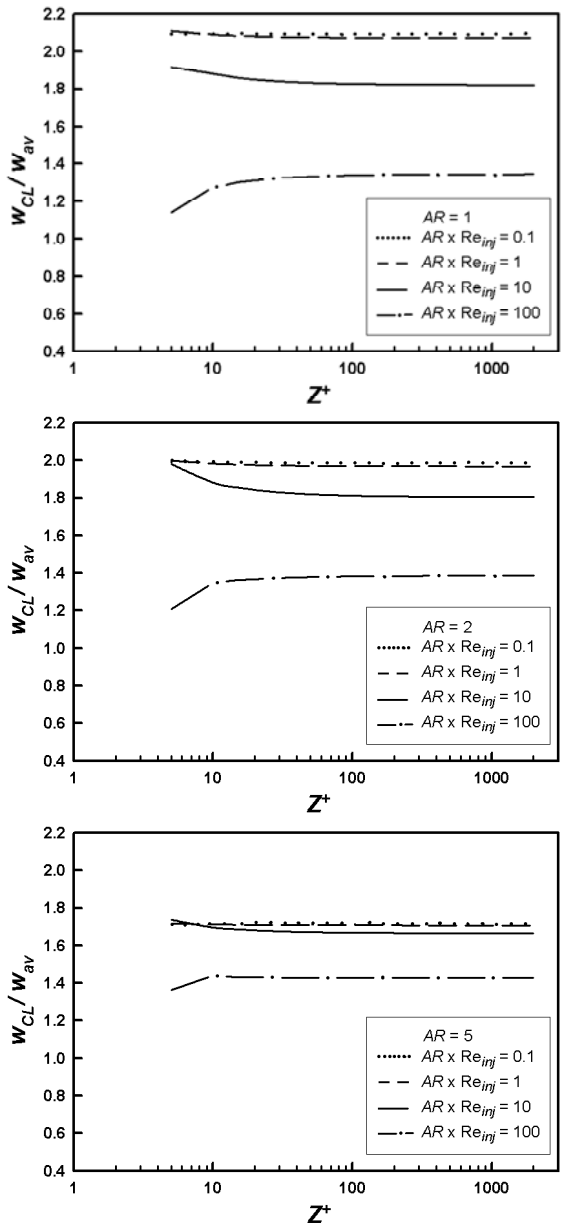

Figure 8: Variation of (w_{CL}/w_{av}) with Z^+.

In the computer simulations using the aforementioned three-dimensional parabolic FVM, in all cases considered, using guidance from the results of the test problems discussed in the previous section, a uniform 41 x 41 nodes grid in the X-Y plane was used. In the longitudinal (z) direction, as was discussed in the previous paragraph, fully-developed conditions are

established after a sufficient distance form the block end (at z = 0). Preliminary trial computations indicated that this fully developed region is essentially established for values of Z^+ greater than 300 (or lower) in each of the 12 cases considered. In this investigation, a uniform axial step size of $\Delta Z^+ = 5$ was used in all of the final numerical simulations. Grid checks done for $AR = 1$ and $AR \times \mathrm{Re}_{inj} = 100$ indicated that this axial step size yields results in the developing region that are within 5% of the essentially grid-independent results: the essentially grid-independent results were computed using the Richardson extrapolation technique.

Axial Velocity Profiles

The variation of (w_{CL}/w_{av}) with Z^+, where w_{CL} is the axial velocity component at the centerline of the duct, is presented in Figure 8 for AR = 1, 2, and 5, and $AR \times \mathrm{Re}_{inj}$ = 0.1, 1, 10, and 100

As is seen from the results in Figure 8, (w_{CL}/w_{av}) achieves essentially constant values for values of Z^+ greater than 300 (or lower) in each of the 12 cases considered. The values of (w/w_{av}) at all other points in the duct cross-section (x-y plane) exhibited similar behavior. These results clearly show the establishment of the fully-developed region that was discussed earlier.

For the duct of square cross-section (AR = 1), the variation of (w/w_{av}) in the vertical longitudinal symmetry surface, (x/b) = 0.5(a/b) = 0.5AR, at four different axial locations, Z^+ = 5, 10, 100, and 1000, are presented in Figure 9 for $AR \times \mathrm{Re}_{inj}$ = 100 (high injection rate). These results show that the (w/w_{av}) profiles are skewed towards the upper wall, (y/b) = 1.0, and become essentially invariant with axial distance for $Z^+ \geq 100$, indicating the establishment of the fully developed region.

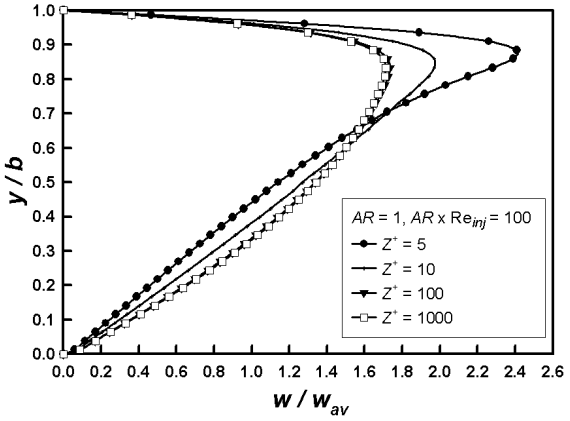

Figure 9: Profiles of (w/w_{av}) in the vertical longitudinal symmetry surface, (x/b) = 0.5(a/b) = 0.5AR, at four different dimensionless axial distances for AR = 1 and $AR \times \mathrm{Re}_{inj}$ = 100.

Table 1: Values of $(f\,\mathrm{Re}_{D_h})_{F.D.}$

AR	$(f\,\mathrm{Re}_{D_h})_{F.D.}$			
	$AR \times \mathrm{Re}_{inj}$			
	0.1	1	10	100
1	57.53	63.39	123.3	639.2
2	62.71	67.59	116.7	573.7
5	76.51	79.16	106.1	385.3

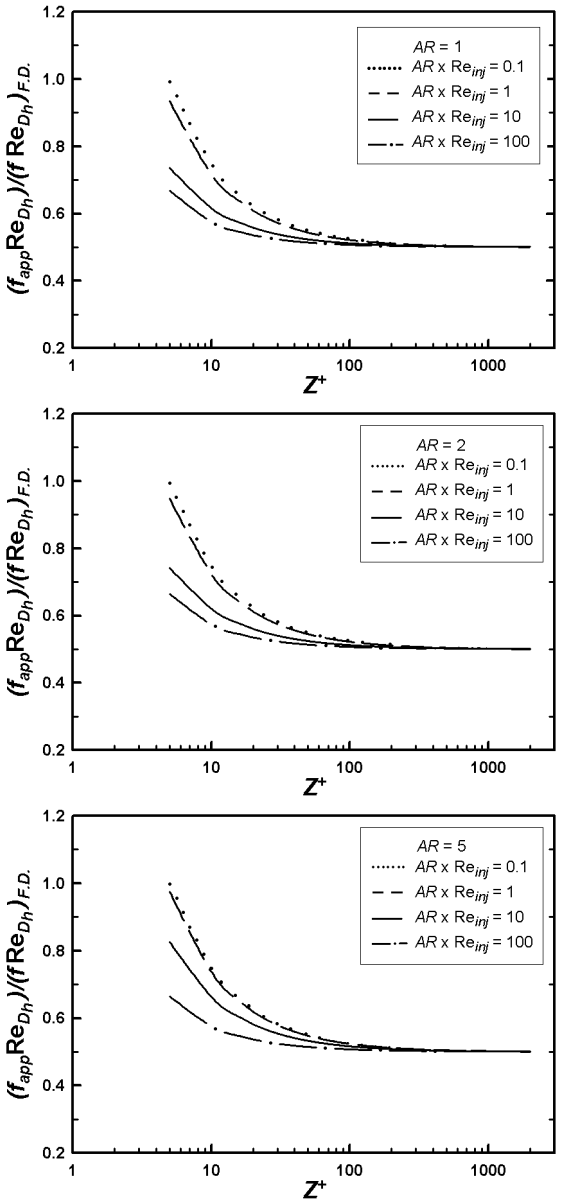

Figure 10: Variation of $(f_{app}\,\mathrm{Re}_{D_h})/(f\,\mathrm{Re}_{D_h})_{F.D.}$ with Z^+.

Friction Factor Values in the Fully-Developed Region

The friction factor is defined as follows [White (1991)]:

$$f = \left\{-(d\bar{P}/dz)D_h\right\} \Big/ \left\{0.5\rho w_{av}^2\right\} \tag{14}$$

In the fully developed region, the product $(f\,\mathrm{Re}_{D_h})_{F.D.}$ becomes a constant. The values of this product for each of the 12 cases considered in this work are presented in Table 1.

The $(f\,\mathrm{Re}_{D_h})_{F.D.}$ values in Table 1 can also be predicted with excellent accuracy using the following correlations (values of the correlation coefficient, R^2, are given along with the correlations):

$$\begin{aligned}
&\text{For } AR = 1: \\
&(f\,\mathrm{Re}_{D_h})_{F.D.} = 5.8309(AR \times \mathrm{Re}_{inj}) + 56.908;\ \mathrm{R}^2 = 0.9997 \\
&\text{For } AR = 2: \\
&(f\,\mathrm{Re}_{D_h})_{F.D.} = 5.118(AR \times \mathrm{Re}_{inj}) + 62.192;\ \mathrm{R}^2 = 0.9999 \\
&\text{For } AR = 5: \\
&(f\,\mathrm{Re}_{D_h})_{F.D.} = 3.0894(AR \times \mathrm{Re}_{inj}) + 76.282;\ \mathrm{R}^2 = 1.0
\end{aligned} \tag{15}$$

Axial Variation of Apparent Friction Factor

The dimensionless reduced pressure *drop* in the duct is expressed in the form of an apparent friction factor as follows:

$$f_{app} = \left\{(\bar{P}_{z=0} - \bar{P}_z)/z\right\} D_h \Big/ \left\{0.5\rho w_{av}^2\right\} \tag{16}$$

Results pertaining to the variation of $(f_{app}\,\mathrm{Re}_{D_h})/(f\,\mathrm{Re}_{D_h})_{F.D.}$ with the dimensionless axial coordinate Z^+ defined in equation (13) are presented in Figure 10, for AR = 1, 2, and 5, and $AR \times \mathrm{Re}_{inj}$ = 0.1, 1, 10, and 100. These results also show the establishment of a full-developed region for values of Z^+ greater than 300 (or lower), with $(f_{app}\,\mathrm{Re}_{D_h})/(f\,\mathrm{Re}_{D_h})_{F.D.}$ asymptoting to the theoretical fully-developed value of 0.5 for all of the cases considered.

CONCLUSION

In this work, a three-dimensional parabolic model of steady, laminar, vapor flow in straight rectangular grooves of flat evaporators used in loop heat pipes (LHPs) was presented first in this paper. Next, an overview of the formulation of a finite volume method (FVM) for the solution of this mathematical model was presented. Following that, the results obtained for 12 different cases for the problem of interest (AR = 1, 2, and 5; and $AR \times \mathrm{Re}_{inj}$ = 0.1, 1, 10, and 100) were presented and discussed. These results clearly show that a fully-developed region is established a sufficient distance downstream of the blocked end of the rectangular duct, for Z^+ greater than 300 (or lower) for the cases considered. The values of $(f\,\mathrm{Re}_{D_h})_{F.D.}$ presented in Table 1, the corresponding correlations given in equation (15), and the $(f_{app}\,\mathrm{Re}_{D_h})/(f\,\mathrm{Re}_{D_h})_{F.D.}$ results presented in Figure 10 (and suitable curve fits to these results, if needed) could be used to enhance the capabilities of current quasi one-dimensional models of LHPS.

ACKNOWLEDGMENTS

Financial sponsorships of this work by the Natural Sciences and Engineering Research Council (NSERC) of Canada, the Fonds québécois de la recherche sur la nature et les technologies (FQRNT), and the Canadian Space Agency (CSA), through doctoral scholarships to the first author and research grants to the second author, are gratefully acknowledged.

REFERENCES

Atabaki, N. (2006), Experimental and Computational Studies of Loop Heat Pipes, *Ph.D. Thesis*, Dept. of Mech. Eng., McGill Univ., Montreal, Quebec, Canada.

Atabaki, N., Jesuthasan, N., and Baliga, B.R. (2007), Steady-state network thermofluid models of loop heat pipes, *Proc. ASME-JSME Thermal Engineering Summer Heat Transfer Conference*, Paper HT2007-32681, pp. 1-11, Vancouver, British Columbia, Canada, July 8-12.

Baliga, B.R. and Atabaki, N. (2006), Control-volume-based finite difference and finite element methods, in *Handbook of Numerical Heat Transfer*, 2nd Ed., W.J. Minkowycz, E.M. Sparrow, and J.Y. Murthy (Editors), Chapter 6, John Wiley & Sons, New York.

Beale S.B. (2005), Mass transfer in plane and square ducts, *Int. J. Heat Mass Transfer*, **48**, pp. 3256-3260.

Beavers, G.S., Sparrow, E.M. and Magnuson, R.A. (1970), Experiments on hydrodynamically developing flow in rectangular ducts of arbitrary aspect ratio, *Int. J. Heat Mass Transfer*, **13**, pp. 689-702.

Berman, A.S. (1953), Laminar flow in channels with porous walls, *J. Appl. Physics*, **24**, pp. 1232-1235.

Bundy, R.D. and Weissberg, H.L. (1970), Experimental study of fully developed laminar flow in a porous pipe with wall injection, *Phys. Fluids*, **13**, pp. 2613-2615.

Busse, C.A. (1967), Pressure drop in the vapor phase of long heat pipes, *Proc. Thermionic Conversion Specialist Conference*, Paolo Alto, California, p. 391.

Busse, C.A. (1973), Theory of the ultimate heat transfer limit of cylindrical heat pipes, *Int. J. Heat Mass Transfer*, **16**, pp. 169-186.

Chen, M.M. and Faghri, A. (1990), An analysis of the vapor flow and the heat conduction through the liquid-wick and pipe wall in a heat pipe with single and multiple heat sources, Int. J. Heat Mass Transfer, **33**, pp. 1945-1955.

Chi, S.W. (1976), *Heat pipe theory and practice: A sourcebook*, Hemisphere, McGraw-Hill, New York.

Curr, R.M., Sharma, D., and Tatchell, D.G. (1972), Numerical predictions of some three-dimensional boundary layers in ducts, *Comp. Methods Appl. Mech. Eng.*, **1**, pp. 143-158.

Faghri, A. (1995), *Heat Pipe Science and Technology*, Taylor & Francis, Washington, DC.

Goldstein, R.J. and Kreid, D.K. (1967), Measurements of laminar flow development in a square duct using laser-Doppler flowmeter, *J. Appl. Mechanics*, **34**, pp. 813-818.

Hwang, G.J., Cheng, Y.C., and Ng, M.L. (1993), Developing laminar flow and heat transfer in a square duct with one-walled injection and suction, *Int. J. Heat Mass Transfer*, **36**, pp. 2429-2440.

Jesuthasan, N. and Baliga, B.R. (2009), A numerical method for three-dimensional parabolic flow and heat transfer in straight ducts of irregular cross section, Computational Thermal Sciences, **1**, pp. 259-288.

Kaya, T. and Hoang, T.T. (1999), Mathematical modeling of loop heat pipes and experimental validation, *J. Thermophys. Heat Transfer*, **13**, pp. 314-320.

Kinney, R.B. (1968), Fully developed frictional and heat-transfer characteristics of laminar flow in porous tubes, *Int. J. Heat Mass Transfer*, **11**, pp. 1393-1401.

Ku, J. and Leidenfrost, W. (1981), Laminar flow in a porous tube with uniform mass injection, *Ingenieur-Archiv*, **51**, pp. 111-126.

Launay, S., Sartre, V., and Bonjour, J. (2007), Parametric analysis of loop heat pipe operation: a literature review, *Int. J. Thermal Sciences*, **46**, pp. 621–636.

Leong, K.C., Liu, C.Y., and Sun, K.H. (1996), Vapor pressure distribution of a flat plate heat pipe, *Int. Comm. Heat Mass Transfer*, **23**, pp. 789-797.

Maydanik, Y.F. (2005), Loop heat pipes, *Applied Thermal Eng.*, **25**, pp. 635-657.

Patankar, S.V. (1980), *Numerical Heat Transfer and Fluid Flow*, McGraw-Hill, New York.

Patankar, S.V. and Spalding, D.B. (1972), A calculation procedure for heat, mass and momentum transfer in three-dimensional parabolic flows, *Int. J. Heat Mass Transfer*, **15**, pp. 1787-1806.

Pederson, R.J. and Kinney, R.B. (1971), Entrance-region heat transfer for laminar flow in porous tubes, Int. J. Heat Mass Transfer, **14**, pp. 159-161.

Raithby, G. (1971), Laminar heat transfer in the thermal entrance region of circular tubes and two-dimensional rectangular ducts with wall suction and injection, *Int. J. Heat Mass Transfer*, **14**, pp. 223-243.

Raithby, G.D. and Knudsen, D.C. (1974), Hydrodynamic development in a duct with suction and blowing, *J. Appl. Mechanics*, **41**, pp. 896-902.

Rhee, S.J. and Edwards, D.K. (1981), Laminar entrance flow in a flat plate duct with asymmetric suction and heating, *Numerical Heat Transfer, Part B: Fundamentals*, **4**, pp. 85-100.

Rhie, C.M. and Chow, W.L. (1983), Numerical study of the turbulent flow past an airfoil with trailing edge separation, *AIAA Journal*, **21**, pp. 1525-1532.

Saabas, H.J. and Baliga, B.R. (1994), A Co-Located Equal-Order Control-Volume Finite Element Method for Multidimensional, Incompressible Fluid Flow – Part I: Formulation, *Num. Heat Transfer, Part B*, **26**, pp. 381-407.

Sebben, S. and Baliga, B.R. (1995), Some Extensions of Tridiagonal and Pentadiagonal Matrix Algorithms, *Num. Heat Transfer, Part B*, **28**, pp. 323-351.

Shah, R.K. and London, A.L. (1978), *Laminar Flow Forced Convection in Ducts*, Advances in Heat Transfer, Supplement 1, Academic Press, New York.

Silverstein, C.C. (1992), *Design and Technology of Heat Pipes for Cooling and Heat Exchange*, Hemisphere, Taylor & Francis, Washington, DC.

Taylor, G. (1956), Fluid flow in regions bounded by porous surfaces, *Proc. Royal Soc. London, Series A, Mathematical and Physical Sciences*, **234**, pp. 456-475.

Tien, C.L. and Rohani, A.R. (1974), Analysis of the effects of vapor pressure drop on heat pipe performance, *Int. J. Heat Mass Transfer*, **17**, pp. 61-67.

Vlassov, V. and Riehl, R. (2008), Mathematical model of a loop heat pipe with cylindrical evaporator and integrated reservoir, *Applied Thermal Eng.*, **28**, pp. 942–954.

Vasiliev, L., Lossouarn, D., Romestant, C., Alexandre, A., and Bertin, Y. (2009), Loop heat pipe for cooling of high-power electronic components, *Int. J. Heat Mass Transfer*, **52**, pp. 301–308.

White, F.M., 1991, *Viscous Fluid Flow*, 2nd Edition, McGraw-Hill, New York.

Yuan, J., Rokni, M., and Sunden, B. (2001), Simulation of fully developed laminar heat and mass transfer in fuel cell ducts with different cross-sections, *Int. J. Heat Mass Transfer*, **44**, pp. 4047-4058.

Yuan, S.W. and Finkelstein, A.B. (1958), Heat transfer in laminar pipe flow with uniform coolant injection, Jet Propulsion, **28**, pp. 178-181.

